



Stiffness reduction factor requirements for the stability analysis of rotary straightened W-shape members

Hyeyoung Koh ¹, Barry T. Rosson ², Hannah B. Blum ³

Abstract

Rotary straightened wide-flange cross-sections are becoming more common in the structural steel industry. The rotary straightening process results in a different residual stress distribution compared to those produced without rotary straightening. The current stiffness reduction factor specified in Chapter C of AISC 360 for stability design does not accurately account for the stiffness reduction of rotary straightened W-shape columns and beam-columns. The beam element stiffness reduction, denoted τ or tau, material model for rotary straightened hot-rolled sections was previously validated and preliminary studies indicated that a different stiffness reduction model is warranted for these shapes compared to the recommended model in AISC 360. This paper presents the results of a parametric study of the current and proposed stiffness reduction models on hot-rolled steel W-shapes. Beam finite element models were created in MASTAN2 and second-order inelastic analyses were conducted. A range of different cross-section geometries typically used for beam-columns were investigated, which includes various flange and web slendernesses and aspect ratios. Columns and beam-columns were investigated with uniaxial bending about the major and minor axes with multiple axial utilization ratios. The effects of the assumed residual stress pattern on the stability limit state are discussed. The results of this sensitivity study are presented along with comparisons and recommendations for further study of the tau stiffness reduction values for hot-rolled steel rotary straightened members.

1. Introduction

The stability design requirements in Chapter C of AISC 360 (2016) applies a stiffness reduction factor τ which accounts for reduced stiffness due to inelasticity for determining the required strength of structural members. This stiffness reduction factor depends only on the utilization ratio of the axial compressive strength of the member. Rosson (2018) developed a nonlinear material model for compact wide-flange sections to improve the existing stiffness reduction model by considering both the axial load and bending moment contributions to stiffness reduction. Three-dimensional $m - p - \tau$ surface plots of W-shapes were assessed to determine the perimeter conditions for m , p , and c_r , where m is a normalized moment, p is the axial utilization ratio, and c_r

¹Graduate Research Assistant, University of Wisconsin-Madison, <hyeyoung.koh@wisc.edu>

²Professor, Florida Atlantic University, <rosson@fau.edu>

³Assistant Professor and Alain H. Peyrot Fellow, University of Wisconsin-Madison, <hannah.blum@wisc.edu>

is the ratio of maximum compressive residual stress to yield stress. The model was calibrated on W-shapes with the ECCS residual stress pattern (ECCS 1984) and validated on several different cross-sections with minor or major axis bending.

Rotary straightened structural steel cross-sections have a different residual stress pattern compared to those without rotary straightening because the rotarizing process removes or significantly reduces the compressive residual stresses at the flange tips. This affects structural behavior especially in members subjected to inelastic buckling. Rosson (2021) made the necessary adjustments to the previously developed stiffness reduction (τ) model (Rosson 2018) to model rotary-straightened hot-rolled steel sections using the residual stress pattern measured by Ge and Yura (2019). The calibrated model for the rotarized W-shapes was validated on limit load analyses of a column and a beam-column subjected to uniaxial bending. The analysis results indicated that the current stiffness reduction model specified in Chapter C of AISC 360 (2016) can result in unconservative W-shape requirements for columns when compared with those obtained using the material model for rotary straightened W-shapes.

This work assesses the cross-section dimensional characteristics of W-shapes that affect the limit load capacity results for the three different material models described above. This study conducted a parametric study of the current and proposed stiffness reduction models on hot-rolled steel W-shapes. A range of W14 and W12 sections were investigated, which have various aspect ratios and element slendernesses. Columns and beam-columns with various member slenderness ratios were analyzed to examine the effect of the stiffness reduction models on the limit loads of structural members. Correlations between the limit loads and geometric parameters were determined to investigate the significant factors that influence the results of each material model.

2. The Stiffness Reduction Models

2.1 Chapter C of AISC 360

Chapter C of AISC 360 (2016), which provides the design requirements for stability of steel structures, determines the required strengths of components with consideration of stiffness reductions due to the inelastic behavior such as the effect of residual stresses and partial yielding of the cross-section. The residual stress distribution (Galambos and Ketter 1959, Fig. 1a), which has a 30% of the yield stress as the maximum compressive residual stress σ_{rc} at the flange tips and uniform tension σ_{rt} in the web, is assumed. σ_{rt} is estimated by $\frac{bt_f}{bt_f+t_w d_w} \sigma_{rc}$, which represents $\frac{A_f}{A_f+A_w} \sigma_{rc}$. A factor of 0.8 is applied to all components in the structure to reflect the reduced stiffness. Additionally, for components whose flexural stiffnesses affect the stability of the structure, an additional factor τ_b is applied to reflect reduced flexural stiffnesses. When the axial utilization ratio is less than or equal to 0.5, τ_b is taken as 1.0, indicating that there is no reduction in flexural stiffness. Otherwise, the additional factor is determined by Eq. 1:

$$\tau_b = 4\left(\alpha \frac{P_r}{P_{ns}}\right) \left[1 - \left(\alpha \frac{P_r}{P_{ns}}\right)\right] \quad (1)$$

where α equals 1.0 for the LRFD method and 1.6 for the ASD method, P_r is a required axial com-

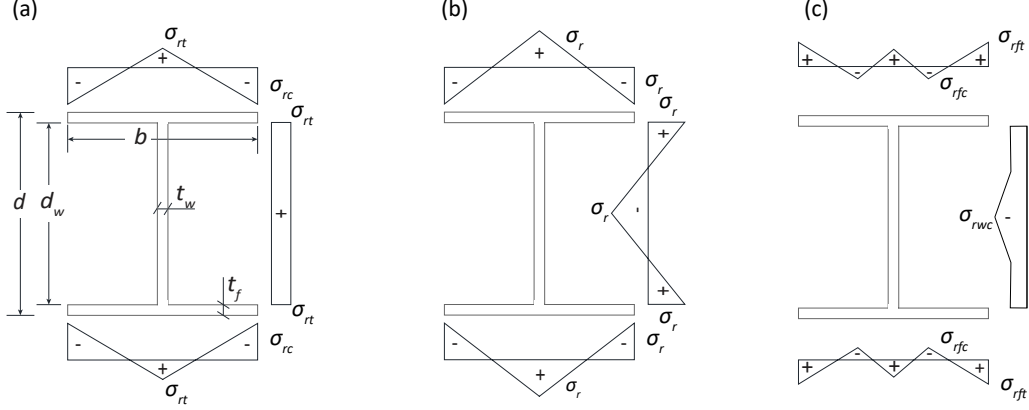


Figure 1: Idealized residual stress models (a) Lehigh (1959) (b) ECCS (1984) (c) Rotary-straightened hot rolled steel section (Ge and Yura 2019)

pressive strength. P_{ns} is the cross-section compressive strength, which equals the yield strength ($\sigma_y \times A_g$) for compact sections. The stiffness reduction relationship is the same regardless of the axis of bending or the presence of bending moment contributing to the loss of flexural stiffness..

2.2 W-shapes with the ECCS residual stress pattern

Rosson (2017) developed a stiffness reduction model for compact W-shapes with an ECCS (1984) residual stress pattern (Fig. 1b), which can consider major axis or minor axis bending. This model will be referred to as “R-ECCS” in the results. As compact doubly-symmetric beam-columns show significantly different behaviors depending on the axis of bending when conducting plastic zone analyses (Attalla et al. 1994, Ziemian and McGuire 2002), the developed model can improve the AISC model by capturing the different responses between major and minor axis bending. The stiffness reduction model is developed based on three-dimensional $m-p-\tau$ surface plots generated by a fiber element model for W-shapes, where m is a moment normalized by plastic moment which is defined as M/M_{px} for major axis bending and M/M_{py} for minor axis bending, p is the applied axial load to yield strength ratio P/P_y , and τ is the stiffness reduction factor. The limit of $\tau = 1.0$ is determined when the m and p conditions generate the sum of three compression stresses equal to the yield stress σ_y , where the compression stresses include the residual compression stress σ_r , the bending moment compression stress σ_m , and the axial compression stress σ_p . The variable p is positive throughout this paper which requires the same sign for P_y and P , where compression is denoted as positive. The maximum moment at which $\tau = 1.0$, denoted $m(\tau = 1.0)$, for major axis bending is given in Eq. 2:

$$m(\tau = 1.0) = \frac{S_x}{Z_x} (1 - c_r - p) \quad (2)$$

where S_x is major axis elastic section modulus and Z_x is major axis plastic section modulus. Eq. 2 is independent of the actual shape of the residual stress pattern because it only considers the maximum residual compressive stress in the flange. The ratio of maximum compressive residual

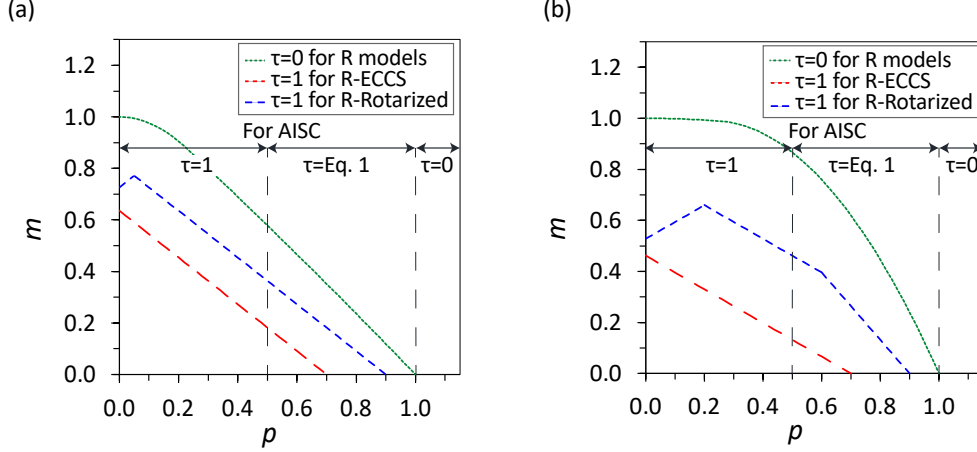


Figure 2: $\tau = 1.0$ and $\tau = 0$ perimeter conditions for W12x65 beam-column with (a) major axis bending (b) minor axis bending

stress at the flange tips to yield stress, c_r , is 0.3 in this study. The maximum moment at which $\tau = 1.0$ for minor axis bending is given in Eq. 3:

$$m(\tau = 1.0) = \frac{S_y}{Z_y}(1 - c_r - p) \quad (3)$$

where S_y is minor axis elastic section modulus and Z_y is minor axis plastic section modulus. Similar to Eq. 2, the actual residual stress pattern does not affect Eq. 3 as it is based on the flange tip compression stress magnitude. Fig. 2 illustrates an example of the $\tau = 1.0$ condition for R-ECCS with major or minor axis bending.

To determine the m condition when $\tau = 0$ (denoted $m(\tau = 0)$) for major axis bending, the required equation is dependent on the plastic neutral axis location in a cross-section. The equation is independent of the shape of the residual stress distribution. Eq. 4 is used when the plastic neutral axis is outside the flange, which is the case for W-shapes under low axial compression loads. Eq. 5 is used for W-shapes under high values of axial compression, when the plastic neutral axis is inside the flange thickness:

$$\text{when } p < \frac{\lambda}{2 + \lambda} \quad m(\tau = 0) = 1 - \frac{p^2(2 + \lambda)^2}{(4\lambda_o + \lambda(4 + \lambda))} \quad (4)$$

$$\text{when } p \geq \frac{\lambda}{2 + \lambda} \quad m(\tau = 0) = \frac{(2 + \lambda_1)^2 - [p(2 + \lambda) - \lambda + \lambda_1]^2}{4 + \lambda_1(4 + \lambda)} \quad (5)$$

where $\lambda = A_w/A_f$ is the ratio of web to flange areas, $\lambda_o = t_w/b_f$ is the ratio of web thickness to flange width, and $\lambda_1 = d_w/t_f$ is the ratio of web depth to flange thickness.

For the minor axis bending condition, Eq. 6 is used when the plastic neutral axis is inside the web, which occurs in wide-flange sections under low values of axial load. Eq. 7 is used for the sections with high axial loads, which have the plastic neutral axis outside the web thickness:

$$\text{when } p < \frac{2\lambda_o + \lambda}{2 + \lambda} \quad m(\tau = 0) = 1 - \frac{p^2(2 + \lambda)^2}{(2 + \lambda\lambda_o)(2 + \lambda_1)} \quad (6)$$

$$\text{when } p \geq \frac{2\lambda_o + \lambda}{2 + \lambda} \quad m(\tau = 0) = \frac{4 - [p(2 + \lambda) - \lambda]^2}{2(2 + \lambda\lambda_o)} \quad (7)$$

The perimeter condition of uniaxial bending when $\tau = 0$ is illustrated in Fig. 2 in addition to the perimeter condition of $\tau = 1$. A τ of 0 indicates that no flexural stiffness remains in the cross-section for the m and p conditions given in Eqs. 6 through 9. The region below the $\tau = 1.0$ line, inside the triangular region, represents the moment and axial load conditions of no stiffness reduction ($\tau = 1.0$). The stiffness reduction factor τ in the region between $\tau = 1.0$ and $\tau = 0$ curves is provided in Eq. 8 and Eq. 9. The values for $m(\tau = 1.0)$ and $m(\tau = 0)$ are determined depending on the axis of bending used to estimate τ :

$$\text{when } p < 1 - c_r \quad \tau = 1 - \left[\frac{m - m(\tau = 1.0)}{m(\tau = 0) - m(\tau = 1.0)} \right]^n \quad (8)$$

$$\text{when } p \geq 1 - c_r \quad \tau = \left[\frac{1 - p}{c_r} \right] \left[1 - \frac{m}{m(\tau = 0)} \right]^n \quad (9)$$

where n is an independent input. This study used n equal to 4 and 2 for major axis bending and minor axis bending, respectively, following Rosson and Ziemian (2019), for modeling W-shapes with the ECCS residual stress pattern.

2.3 Rotary-straightened W-shapes

Rosson (2021) developed a stiffness reduction model for rotary-straightened W-shapes based on the residual stress pattern (Fig. 1c) examined by Ge and Yura (2019). In contrast to the ECCS pattern, which has the maximum compressive residual stresses (σ_{rfc}) at the flange tips, rotary-straightened sections have the maximum residual tensile stresses (σ_{rft}) at the flange tips. This will result in different initial yield load conditions. The maximum compression residual stresses of rotary-straightened sections occur at the quarter-point of the flanges with a reduced magnitude compared to the sections without the rotary-straightening process. The equations for maximum moment $m(\tau = 1.0)$ in Eq. 2 and Eq. 3 are modified to consider this different residual stress pattern of rotary-straightened W-shapes. The maximum moment when $\tau = 1.0$, denoted $m(\tau = 1.0)$, prior to flange initial tension yield under low axial compression conditions for major axis bending is given in Eq. 10 :

$$\text{when } p \leq \frac{c_r^+ - c_r^-}{2} \quad m(\tau = 1.0) = \frac{S_x}{Z_x}(1 - c_r^+ + p) \quad (10)$$

where c_r^+ is the ratio of maximum tensile residual stress σ_{rft} to σ_y and c_r^- is the ratio of maximum compressive residual stress σ_{rfc} to σ_y . This study used $c_r^- = 0.1$ and $c_r^+ = 0.2$ based on the values $\sigma_{rfc} = 5 \text{ ksi}$ and $\sigma_{rft} = 10 \text{ ksi}$ estimated by Ge and Yura (2019). Eq. 11 is used for the maximum moment prior to flange initial compression yield under medium and high axial compression conditions for major axis bending.

$$\text{when } \frac{c_r^+ - c_r^-}{2} < p \leq 1 - c_r^- \quad m(\tau = 1.0) = \frac{S_x}{Z_x}(1 - c_r^- - p) \quad (11)$$

An example of the maximum m and p conditions without stiffness reduction for rotary-straightened sections with major axis bending is shown as $\tau = 1.0$ of R-Rotarized in Fig. 2a. The region below the $\tau = 1.0$ curve indicates that there is no stiffness reduction while the solid curve represents the $\tau = 0$ condition.

For beam-columns under minor axis bending, the maximum moment prior to initial tension yield under low axial compression conditions is determined by Eq. 12. The maximum moment prior to initial compression yield under moderate or high axial compression conditions is determined using Eq. 13 or Eq. 14, respectively. The m and p conditions when $\tau = 1$, defined in Eq. 12 - 14, are illustrated in Fig. 2b as $\tau = 1.0$ of R-Rotarized.

$$\text{when } p \leq c_r^+ \quad m(\tau = 1.0) = \frac{S_y}{Z_y}(1 - c_r^+ + p) \quad (12)$$

$$\text{when } c_r^+ < p \leq 1 - 2c_r^- + c_r^+ \quad m(\tau = 1.0) = \frac{S_y}{Z_y}(1 + c_r^+ - p) \quad (13)$$

$$\text{when } 1 - 2c_r^- + c_r^+ < p \leq 1 - c_r^- \quad m(\tau = 1.0) = \frac{2S_y}{Z_y}(1 - c_r^- - p) \quad (14)$$

Using the calculated $m(\tau = 1.0)$, Eqs. 8 - 9 are used to determine the stiffness reduction τ , where c_r^- is used for c_r in Eq. 9. The n values of 1.5 and 1.2 are used for major axis bending and minor axis bending, respectively, following Rosson (2021), for modeling rotary-straightened W-shapes.

3. Parametric study model inputs

This section presents the inputs for the finite element based parametric study, including stiffness reduction models, geometric properties, and the finite element model details.

3.1 Stiffness reduction models

The three stiffness reduction models presented in previously are considered in the parametric study and are shown in Table 1.

Table 1: Stiffness reduction models

Name	Stiffness reduction model	Assumed residual stress pattern	Equations
AISC	AISC 360 (2016)	Lehigh (1959)	Eq. 1
R-ECCS	Rosson (2017)	ECCS (1984)	Eqs. 2 - 9
R-Rotarized	Rosson (2021)	Ge and Yura (2019)	Eqs. 8 - 14

3.2 Geometric properties

A range of W14 and W12 sections were selected with varying geometric properties. This study selected the relevant geometric ratios which are known to govern the behavior of W-shapes. The geometric ratios considered in the study are:

1. Member slenderness, L/r , where L is the member length and r is r_x or r_y depending on the axis of bending
2. Aspect ratio, b/d , which is the ratio of section width to total section depth. Aspect ratios closer to 1 indicate a square footprint which are more common for columns, while smaller aspect ratios indicate a rectangular footprint which are more common for beams. The b/d effect is considered in a yield surface equation for doubly symmetrical steel sections (Duan and Chen 1990).
3. The ratio of flange-to-web-area, A_f/A_w , where A_f is the flange area and A_w is the web area. This ratio significantly affects the distribution of residual stresses (Schaper et al. 2022). The ratio of web-to-flange area (A_w/A_f) is considered in a yield surface equation for W-shapes

under minor axis bending (Duan and Chen 1990). This is equal to the $\frac{1}{\lambda}$ value presented in Rosson (2018).

4. Flange element slenderness, $b_f/2t_f$, which is half the flange width divided by the flange thickness
5. Web element slenderness, d_w/t_w , which is the web depth between the flanges divided by the web thickness
6. Flange element restraint, b_f/t_w , which reflects how the web restrains the flange element. Consider a constant b_f – a larger b_f/t_w indicates that the web is less thick and hence provides a reduced edge support to the flange than a thicker web which would produce a smaller b_f/t_w value. Hence a larger b_f/t_w value indicates that the flange element is more prone to local buckling. This is equal to the $\frac{1}{\lambda_0}$ value presented in Rosson (2018).

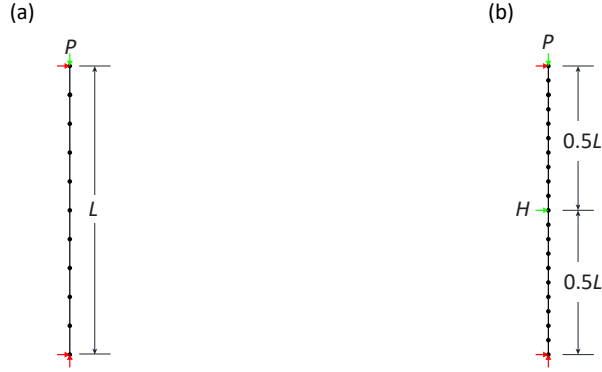


Figure 3: (a) Column model (b) Beam-column model

7. Web element restraint, d_w/t_f , which reflects how the flange restrains the web element. Consider a constant d_w – a larger d_w/t_f indicates that the flange is less thick and hence provides a reduced edge support to the web than a thicker flange which would produce a smaller d_w/t_f value. Hence a larger d_w/t_f value indicates that the web element is more prone to local buckling. This is equal to the λ_1 value presented in Rosson (2018).

3.3 Finite element model

Beam element FE models were created in MASTAN2 (2019), and second-order inelastic analyses were conducted. The steel material was defined with a yield stress of 50 ksi and Young’s modulus of 29,000 ksi. The FE models are restrained from out-of-plane behavior, and all of the members in the study were fully compact per AISC Section B4 definition. Columns and beam-columns were investigated with the applied load condition of axial compression for columns and combined axial compression and uniaxial bending about the major or minor axis for beam-columns. The limit load capacities of steel members were evaluated by using the 0.8τ values determined by Eq. 1 for the AISC model. The R-ECCS model applied τ obtained from Eqs. 3-9. The R-Rotarized model employed Eqs. 8-14 to derive the τ values.

4. Results

4.1 Columns

Limit load analyses on steel columns were first investigated to observe the effect of the stiffness reduction models on the load capacity between two different cross-sections, W14x48 and W14x550. Fig. 3a illustrates a pinned-pinned column that consists of ten line elements and the initial geometric imperfections of $L/1000$ at mid-height. An axial load P was incrementally applied until the column reached the ultimate load. Member slenderness ratios, L/r , in the inelastic range including 40, 60, 80, and 100 were explored in the column models, where r is the radius of gyration of a cross-section. Either r_x (major) or r_y (minor) is used depending on the axis of bending to calculate the length of the member.

Fig. 4 shows the column strength results of the W14x48 and W14x550 members bending about ei-

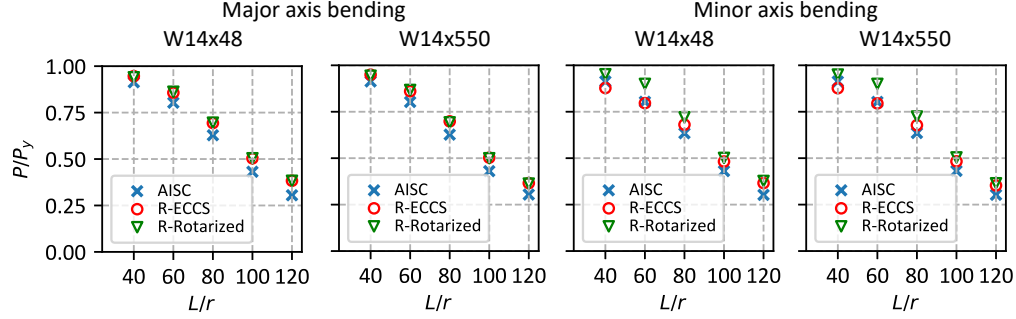


Figure 4: Column strength results of W14x48 and W14x550

ther the major or minor axis. These two sections, which have substantially different cross-sectional properties, were selected to examine if the various stiffness reduction models had different results depending on the cross-section geometry. The column strengths when using the AISC material model are unaffected by major axis or minor axis bending, while the R-ECCS and R-Rotarized models produced different ultimate P/P_y values because these models explicitly considered the axis of bending and residual stress patterns. When comparing the results of W14x48 and W14x550, there are no significant differences between the two cross-sections. This indicates that the application of the stiffness reduction models are negligibly affected by cross-sectional properties. The largest percent difference between the two members is 3.1%, which occurred when using the R-Rotarized model with the $L/r = 100$ column for bending about the minor axis. For major axis bending, the largest percent difference is 2.6% for the $L/r = 80$ column with the R-ECCS model.

In the full range of L/r with major axis bending, the AISC model showed lower strength values compared to the R-ECCS and R-Rotarized models. R-ECCS and R-Rotarized showed almost equal results for both W14 sections. For minor axis bending, the AISC model showed lower estimates compared to the R-ECCS model for columns with $L/r \leq 60$. Moreover, the capacity difference between R-ECCS and R-Rotarized showed the maximum percent difference of 12.2% for $L/r = 60$. The results for minor axis bending are more sensitive to the assumed residual stress pattern than those for major axis bending. Therefore, it is crucial to use the correct residual stress assumption when using the stiffness reduction factor in particular for minor axis bending based on the results of Fig.4.

4.2 Beam-column

This section investigates beam-columns under uniaxial bending with a range of different cross-section geometries including aspect ratio, flange-to-web area ratio, flange and web element slendernesses, and flange and web element restraints. Eight W14 shapes and six W12 shapes were evaluated to determine if the W-shapes commonly used in structural design show similar behaviors among the various stiffness reduction models. The geometric parameters of the selected W-shapes are listed in Table 2. The beam-column model illustrated in Fig. 3b was utilized and member slenderness L/r ranged between 40 to 120 with increments of 20. An initial geometric imperfection of a half sine wave with an amplitude of $L/1000$ at the mid-height of members was modeled. Multi-

Table 2: Selected W-shapes and cross-sectional properties

Section	b/d	A_f/A_w ($1/\lambda$)	$b_f/2t_f$	d_w/t_w	b_f/t_w ($1/\lambda_0$)	d_w/t_f (λ_1)
W14x48	0.58	1.11	6.75	33.60	23.62	21.19
W14x61	0.72	1.34	7.75	30.40	26.67	19.55
W14X82	0.71	1.36	5.92	22.40	19.80	14.73
W14x109	1.02	1.90	8.49	21.70	27.81	14.63
W14x283	0.96	2.06	3.89	8.84	12.48	6.07
W14x550	0.85	2.09	2.25	4.79	7.23	3.29
W14x605	0.83	2.20	2.09	4.39	6.69	3.02
W14x873	0.80	2.21	1.71	2.89	4.77	2.28
W12x50	0.66	2.56	6.30	26.80	21.84	17.06
W12x72	0.98	3.41	9.00	22.60	27.91	16.36
W12x96	0.96	3.66	6.80	17.70	22.18	12.11
W12x152	0.91	3.69	4.50	11.20	14.37	7.80
W12x230	0.85	3.78	3.10	7.56	10.00	5.29
W12x336	0.80	4.10	2.30	5.47	7.53	3.68

ple axial utilization ratios p of 0.3, 0.5, and 0.7 were applied to the beam-columns. The axial load P corresponding to $p \times 50$ ksi was first applied and then the horizontal load H was incrementally applied until the beam-column reached the limit load.

Correlation relationships between the geometric parameters and the normalized load capacity of the W14 beam-columns were explored for all of the axial loading, bending, and member slenderness conditions. The limit load was normalized to $H/(F_y Z)$, where Z is plastic section modulus; either Z_x or Z_y depending on the axis of bending, major or minor, respectively. The Pearson's correlation coefficient ρ given in Eq. 15 was utilized to measure a linear correlation:

$$\rho = \frac{cov(X, Y)}{\sigma_X \sigma_Y} \quad (15)$$

where cov is the covariance, σ_X is the standard deviation of a variable X , which is the normalized limit load obtained from analyses, and σ_Y is the standard deviation of a variable Y , a geometric parameter such as b/d , A_f/A_w , $b_f/2t_f$, d_w/t_w , b_f/t_w , and d_w/t_f . This study assumed the correlation was strong when the correlation absolute value was greater than 0.9.

The scatter plots of the normalized capacity of the $L/r = 40$ beam-columns versus the geometric parameters for major axis bending are illustrated in Fig. 5. A slenderness ratio of 40 was selected because it is in the inelastic buckling range where residual stresses are most influential on member capacity and where significant yielding of a cross-section can occur at failure. The correlation coefficients for each stiffness reduction model are given in the legend. The scatter plots of flange and web element restraints (b_f/t_w and d_w/t_f) were excluded because they showed almost the same correlation values with element slendernesses, $b_f/2t_f$ and d_w/t_w , respectively. This is due to the nearly perfect correlation between t_f and t_w as shown in Fig. 6. For all p conditions, the AISC model resulted in a consistent normalized capacity over the range of all parameters, while the capacities of the other models varied over the range of all parameters. AISC has the lowest limit

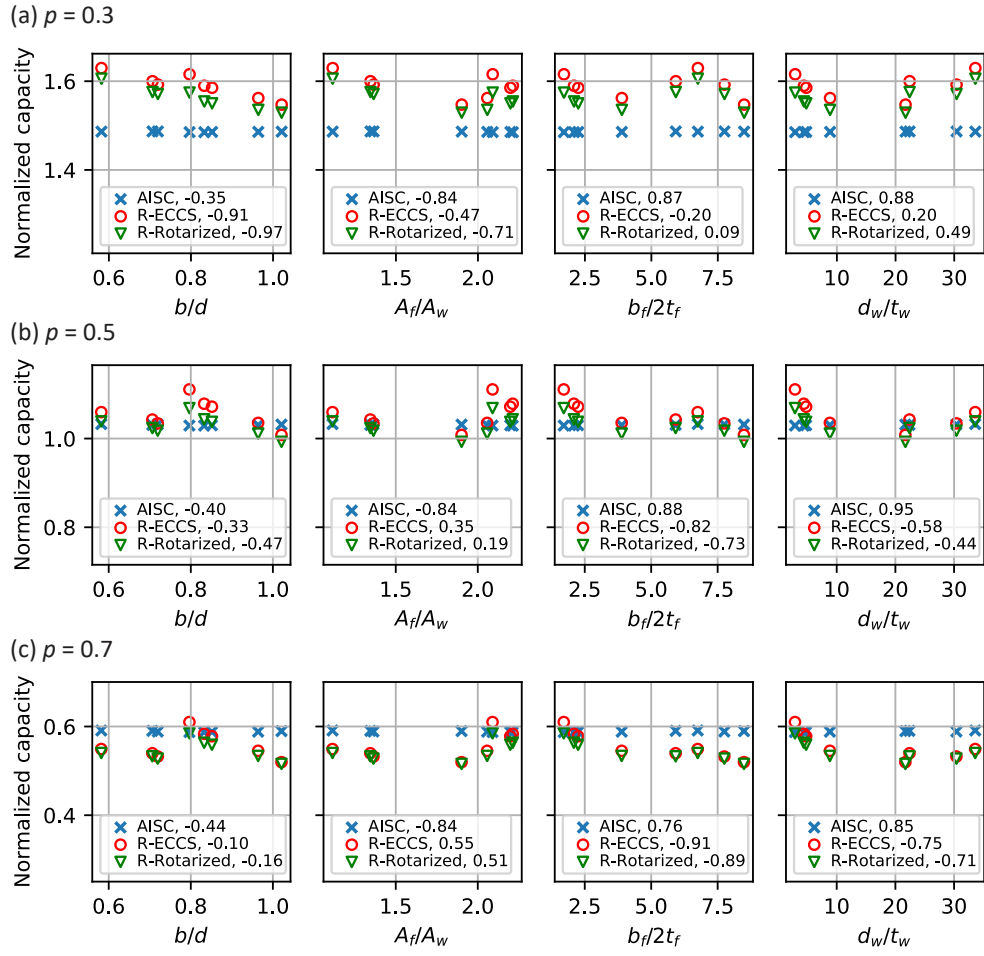


Figure 5: Scatter plots of the capacity of the $L/r = 40$ beam-column with major axis bending versus geometric properties when (a) $p = 0.3$, (b) $p = 0.5$, and (c) $p = 0.7$

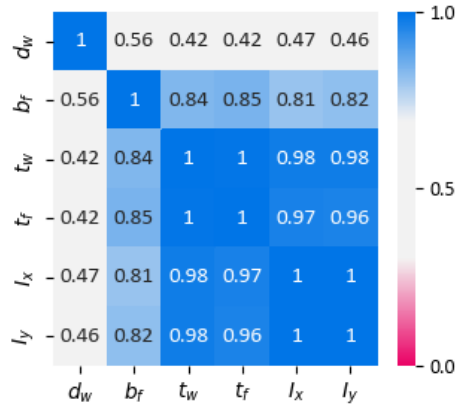


Figure 6: Correlation matrix within the cross-sectional geometries

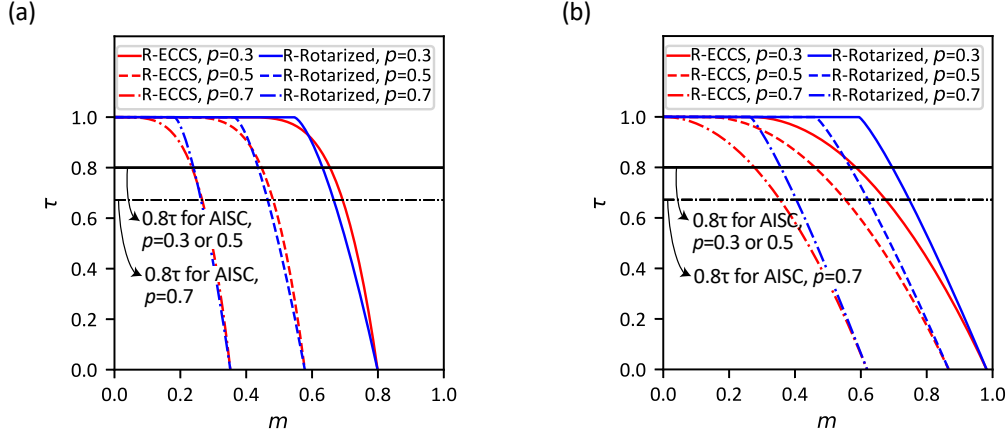


Figure 7: $\tau - m$ relationships when $p = 0.3$, $p = 0.5$, and $p = 0.7$ with (a) major axis bending (b) minor axis bending

load under the low axial load condition $p = 0.3$ out of the three models. For medium axial load, $p = 0.5$, all models capacities are more closely aligned. For high axial load, $p = 0.7$, the AISC model provides a higher normalized load prediction relative to R-ECCS and R-Rotarized models. As shown in Fig. 7a, AISC applies the same value of the stiffness when $p = 0.3$ and $p = 0.5$ while the other models use the τ values that rapidly decrease as p and m increase. Therefore, the capacities of R-ECCS and R-Rotarized decrease with increased p and m compared to AISC capacities. For the major axis bending condition in Fig. 7a, R-Rotarized has slightly lower τ values compared with R-ECCS except near the initiation of stiffness reduction near $\tau = 1.0$. However in Fig. 7b, for the minor axis bending condition, R-Rotarized has consistently higher tau values compared with R-ECCS. As illustrated in Fig. 5c, the AISC model gives unconservative capacities compared with the other models for the $p = 0.7$ condition. This indicates that for high axial load conditions of beam-columns, the material model used in the analysis should be based on stiffness reduction that is based on both m and p .

Fig. 8 shows the scatter plots of the $L/r = 40$ beam-columns with minor axis bending. The AISC model again showed consistent load capacities over the range of geometric parameters. Overall, the capacity difference between the R-ECCS and R-Rotarized models is larger than for major axis bending due to the significantly different shape of the plateau when $\tau = 1.0$ for minor axis bending. As previously discussed in Section 3.1, R-ECCS applies one linear function for the maximum moment when $\tau = 1.0$, but R-Rotarized involves three different $m(\tau = 1.0)$ equations depending on the p magnitudes. As shown in Fig. 7b, the $\tau - m$ curves of R-ECCS and R-Rotarized have a significant gap because of the large $\tau = 1.0$ plateau of the R-Rotarized model. AISC highly overestimated the limit load relative to the other models at higher values of p , which results in unconservative capacity predictions. When using the AISC model, the ultimate capacity of steel members and frames under minor axis bending can be overestimated especially at high axial load ratios. The overpredicted capacity by AISC emphasizes the need to consider an appropriate residual stress pattern for hot-rolled and rotary-straightened sections in steel stability analysis.

Fig. 9 summarizes the correlation coefficients of the W14 beam-column capacities having L/r ranging from 40 to 120 and p from 0.3 to 0.7. In some cases, the beam-columns reached the limit

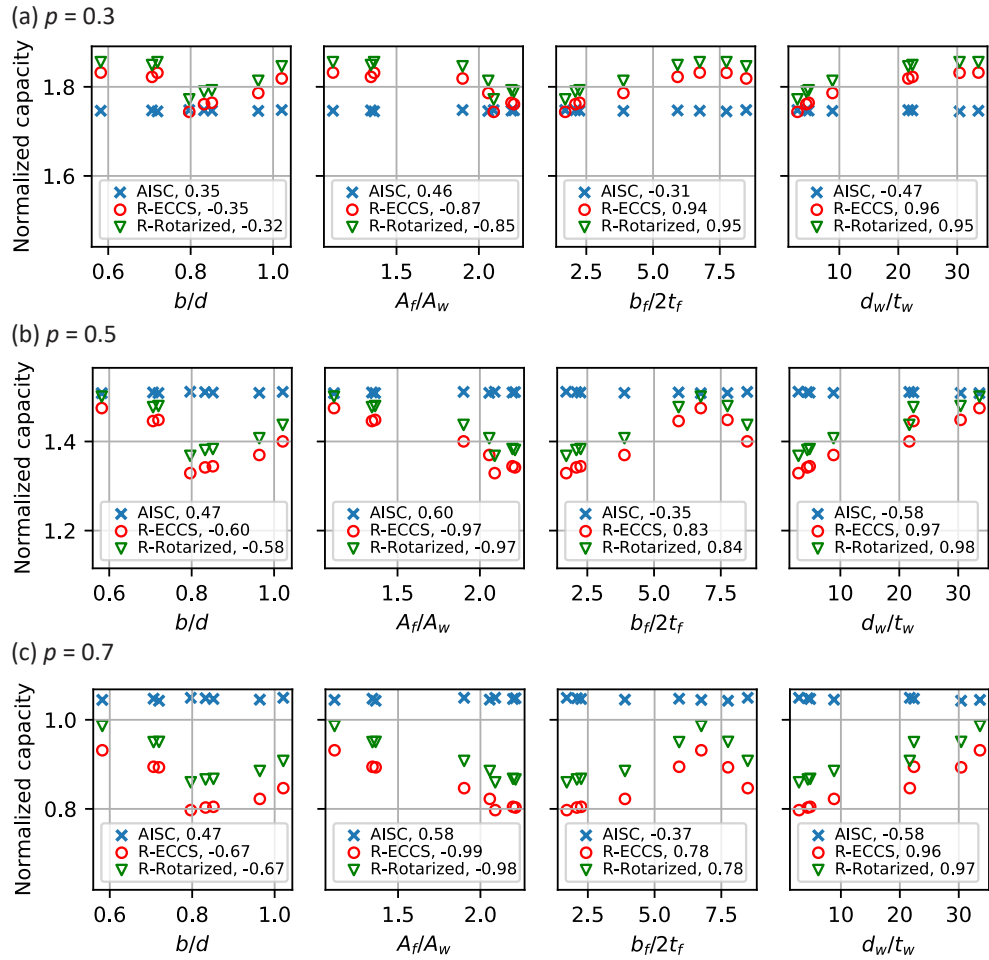


Figure 8: Scatter plots of the capacity of the $L/r = 40$ beam-column with minor axis bending versus geometric properties when (a) $p = 0.3$, (b) $p = 0.5$, and (c) $p = 0.7$. The numbers in the legend indicate the correlation coefficients.

load prior to the full application of p . This situation was more prevalent with the AISC model than the R-ECCS and R-Rotarized models. The blue contoured cells indicate a positive correlation between the normalized load capacity and the parameters, while the red-colored cells indicate a negative relationship. The parameters were described in Section 3.2.

For major axis bending, most parameters in the AISC model are shown to have a high correlation with the capacity. This is visible if the plots in Fig. 5 are greatly magnified. However, the AISC capacity showed a difference of less than 0.003 over the range of parameters while the R- models had a difference of 0.8, which indicates a negligible change in the AISC results (Fig. 5). Therefore, it is difficult to justify that the magnitude of the geometric parameters is sensitive to the AISC model. In general, R-ECCS and R-Rotarized are strongly influenced by b/d under low axial loads ($p = 0.3$) especially for $L/r < 100$. As shown in Fig. 7a, the $p = 0.3$ condition has small or no stiffness reduction over a wide range of m from 0 to 0.6. Without the stiffness reduction, the cross-section can support more load before failure, which could result in parts of the cross section reaching the yield strength. Under major axis bending, the flanges resist the applied bending, and as such the aspect ratio, b/d , influences the strength under low p . Considering the residual stresses in W-shapes, flanges reach the yield limit earlier than a web under low axial compression loads. As such, a beam-column with low p can deliver a larger rotation capacity than for the case of high axial load. As p increases, the web yields with the flange, thus the web properties (d_w/t_w and d_w/t_f) have a large correlation as p increases for both R-ECCS and R-Rotarized. Additionally, the flange properties ($b_f/2t_f$ and b_f/t_w) are shown to have a large effect for $L/r \leq 60$, indicating that residual stress is more significant than member slenderness. Although the effect of residual stresses is important for small L/r , the effect of A_f/A_w on the R-ECCS results for low L/r is not significant because the ECCS pattern (Fig. 1b) has the same amount of compression area on the flanges regardless of the shapes. For $L/r \geq 80$ with the R-Rotarized model, A_f/A_w , d_w/t_w , and d_w/t_f have a strong correlation with the capacity. Since rotary-straightened sections have the compressive residual stress along with the web (Fig. 1c), the web has a significant effect on the slender members that are affected by bending.

For minor axis bending, all of the parameters have weak correlations with the capacity predicted by AISC while R-ECCS and R-Rotarized show that most parameters except b/d have a strong effect on the capacity. According to the R-ECCS and R-Rotarized results, web element slenderness d_w/t_w and web element restraint d_w/t_f are shown to be significant in all of the L/r and p conditions, which indicates the importance of the web related parameters in the minor axis bending behavior. Moreover, flange element slenderness $b_f/2t_f$ and flange element restraint b_f/t_w have a high impact on the member capacity under the low axial load condition but the impact reduces under higher axial loads. For W-shapes with minor axis bending, initial yielding occurs only at the flange tips (Kucukler et al. 2014). This indicates that the effect of flange element characteristics is more influential in the low axial load conditions. A_f/A_w is shown to have a strong correlation over the range of L/r . This reflects that W-shapes with minor axis bending are more sensitive to the distribution of areas (A_w/A_f) in a cross-section for major axis bending (Santathadaporn and Chen 1970). Moreover, as a large A_f/A_w leads to a low bending moment capacity due to an increased area distributed far away from the centroidal axis (Duan and Chen 1990), A_f/A_w has a negative correlation with the capacity.

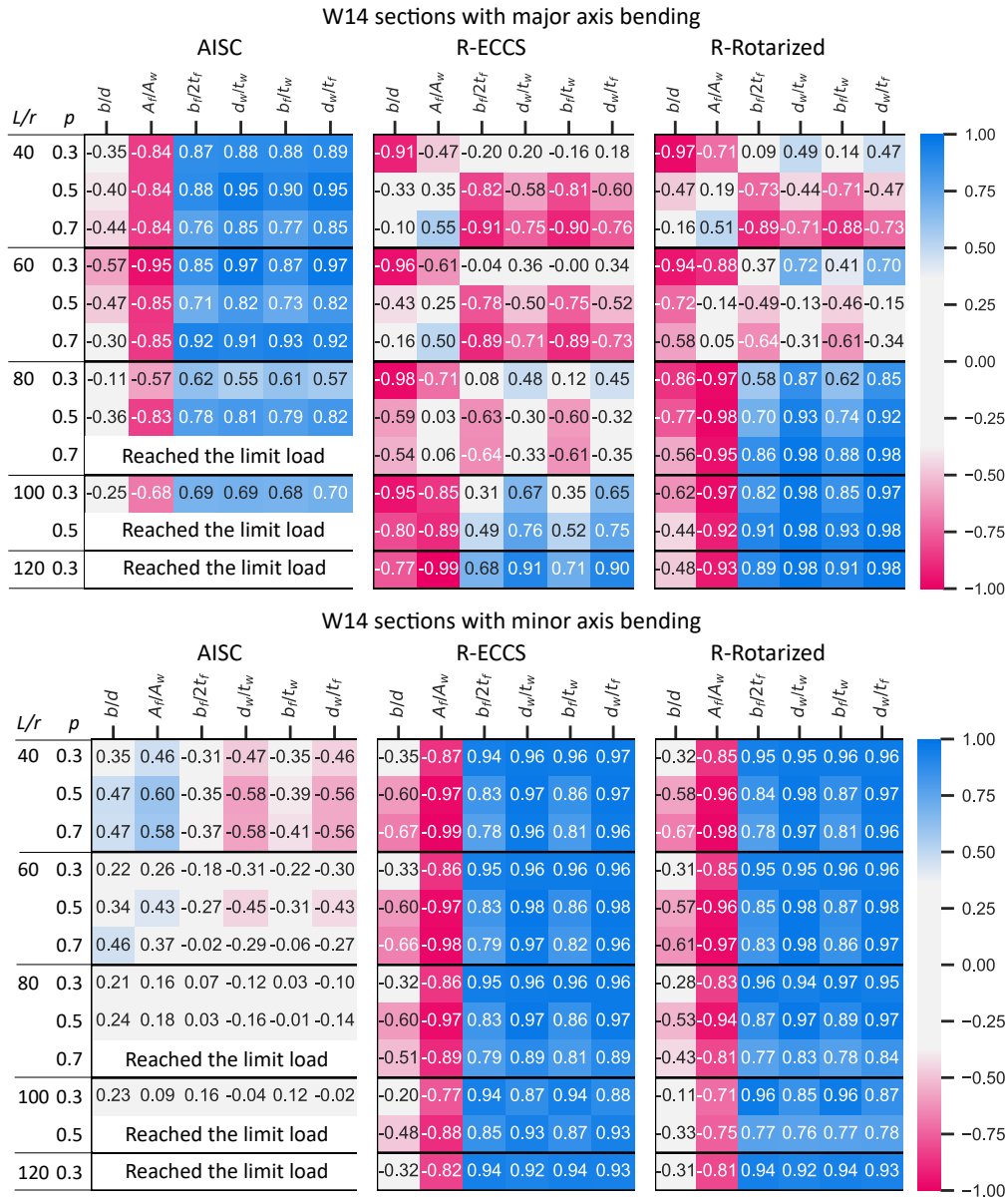


Figure 9: Correlation values of the W14 beam-columns with major axis bending (top row) and minor axis bending (bottom row). Blue = positive correlation, Red = negative correlation.

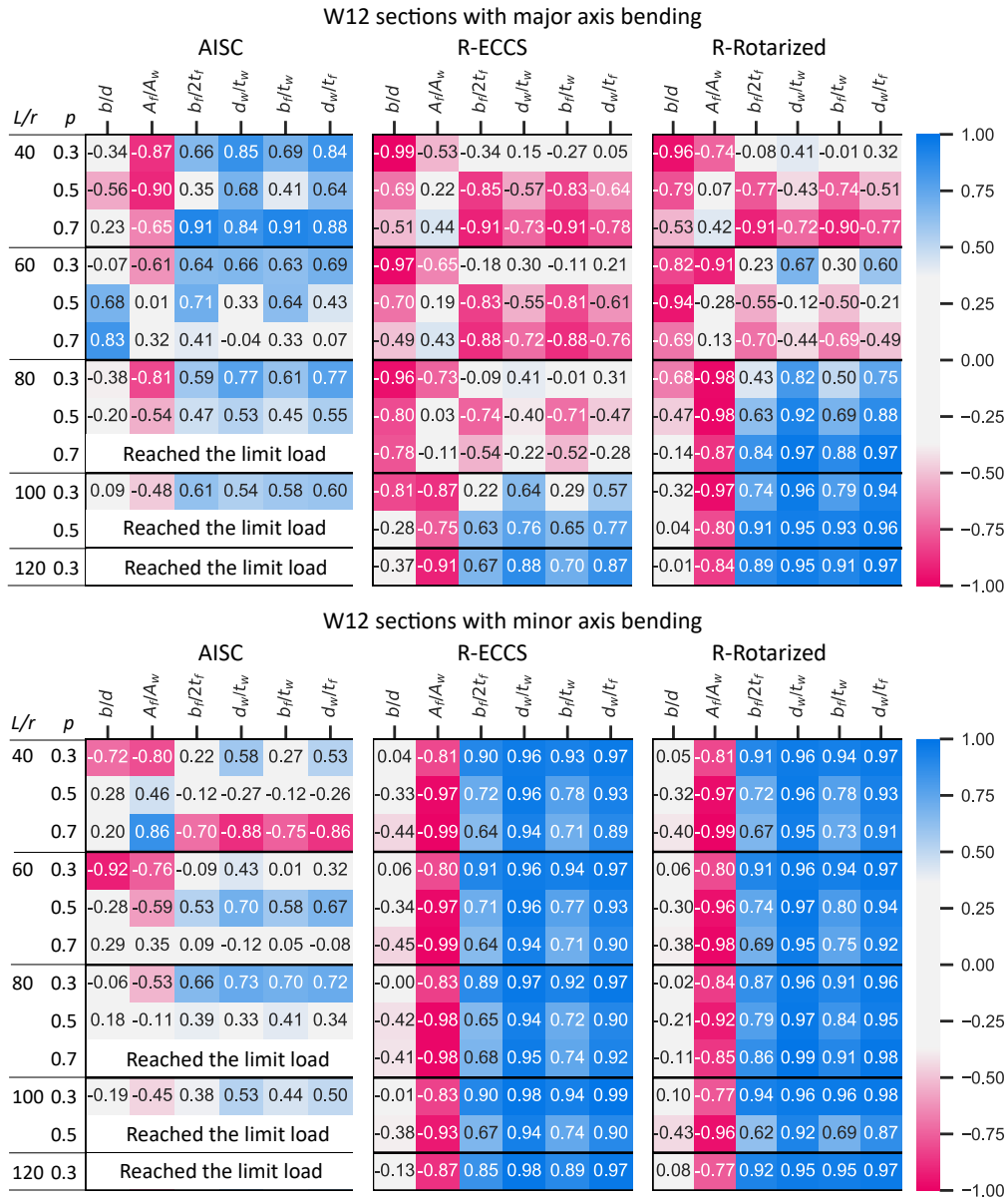


Figure 10: Correlation values of the W12 beam-columns with major axis bending (top row) and minor axis bending (bottom row)

Six W12 sections listed in Table 2 were investigated, and the correlation results are summarized in Fig. 10. The correlation patterns of the W12 sections are overall similar to those of the W14 shapes, which supports the findings of W14 analysis. For example, the AISC results are not sensitive to the magnitude of geometric parameters for both major and minor axis bending. For R-ECCS and R-Rotarized with major axis bending, different parameters have a high correlation value depending on the member slenderness ratio L/r and axial load conditions p . The minor axis bending results indicate that the web parameters are critical over the ranges of L/r and p , and the flange parameters are sensitive to the members under low axial loads. There are no notable differences between the results for the W12 and W14 members.

5. Conclusions

A beam-element based parametric study on hot-rolled wide-flange sections was conducted. Three different stiffness reduction models were investigated, including the current model specified in AISC 360 (2016), a model for hot-rolled W-shapes with the ECCS (1984) residual stress pattern, and a model for rotary-straightened W-shapes with the residual stress pattern provided by Ge and Yura (2019). Various compact W12 and W14 shapes were employed to examine the effect of multiple cross-sectional parameters on the limit load of columns and beam-columns with a range of slenderness ratios and axial utilization ratios. For columns, it was shown that overall the AISC model resulted in lower strength values than the ECCS and rotary-straightened models. This difference was larger for columns bending about their minor axis than their major axis. For beam-columns, it was shown that overall the AISC model predicts a lower load capacity under low axial loads and a higher load capacity under high axial loads than both the ECCS and rotary-straightened models. This may result in conservative load predictions for AISC beam-columns under low axial load, and more importantly, an unconservative load prediction for AISC beam-columns under high axial load. The overpredictions by the AISC model also occurred in intermediate axial load levels for beam-columns with minor axis bending. The AISC model was not sensitive to the magnitude of geometric parameters for both major and minor axis bending because of the simplified equation for the stiffness reduction factor while the models that incorporate residual stress patterns of ECCS and rotary-straightened W-shapes have different influential factors depending on the values of axial utilization ratio and member slenderness ratio. The results of the study indicate that it is necessary to include an appropriate residual stress distribution to accurately examine the effect of reduced stiffness for steel stability analysis.

6. Future work

Future studies may include frame analyses to examine the effect of the stiffness reduction models on system behaviors. Since beam-columns with major or minor axis bending had different cross-section dimensional characteristics that affect the limit load capacity, the bending axis conditions should be considered in the frame analysis. In addition, model validation studies on previous experimental data for columns and beam-columns can be conducted. Since rotary-straightened W-shapes are commonly used in the construction industry, the study would help determine an appropriate stiffness reduction factor systems with these members. Lastly, elaborate frame models such as three-dimensional shell FE models can be developed to examine the effect of residual stresses on behaviors of rotary-straightened sections in detail.

Notation

A_g	=	Gross area
A_f	=	Flange area
A_w	=	Web area
E	=	Elastic modulus
H	=	Lateral load
L	=	Member length
M_p	=	Plastic moment
P	=	Axial load
P_y	=	Cross-section yield strength
P_r	=	Required axial compressive strength
S	=	Elastic section modulus; S_x is used for major axis bending and S_y is used for minor axis bending
Z	=	Plastic section modulus; Z_x is used for major axis bending and Z_y is used for minor axis bending
b	=	Flange width
c_r	=	Ratio of maximum compressive residual stress to yield stress presented in Rosson (2017)
c_r^+	=	Ratio of the maximum tensile residual stress (σ_{rft}) to yield stress (σ_y) presented in Rosson (2021). Positive value is used for Eqs. 10-14
c_r^-	=	Ratio of the maximum compressive residual stress (σ_{rfc}) to yield stress (σ_y) presented in Rosson (2021). Positive value is used for Eqs. 10-14
d	=	Cross-section depth
d_w	=	Web depth
m	=	Normalized moment
$m(\tau = 0)$	=	m value when $\tau = 0$
$m(\tau = 1.0)$	=	m value when $\tau = 1.0$
p	=	P/P_y , the applied axial load to yield strength ratio
r	=	Radius of gyration; r_x is used for major axis bending and r_y is used for minor axis bending
t_f	=	Flange thickness
t_w	=	Web thickness
λ	=	Ratio of web to flange areas (A_w/A_f)
λ_o	=	Ratio of web thickness to flange width (t_w/b_f)
λ_1	=	Ratio of web depth to flange thickness (d_w/t_f)
ρ	=	Correlation coefficient
σ_r	=	Maximum residual stress for the ECCS pattern (1984)
σ_{rc}	=	Maximum compressive residual stress for the Lehigh pattern (1959)
σ_{rt}	=	Maximum tensile residual stress for the Lehigh pattern (1959)
σ_{rft}	=	Maximum tensile residual tension in flanges for rotary-straightened sections (Ge and Yura 2019)
σ_{rfc}	=	Maximum compressive residual stress in flanges for rotary-straightened sections (Ge and Yura 2019)

- σ_{rwc} = Maximum compressive residual stress in a web for rotary-straightened sections (Ge and Yura 2019)
- σ_y = Yield stress
- τ = Stiffness reduction factor

References

- AISC (2016). *Specification for Structural Steel Buildings ANSI/AISC 360-16*. Chicago, IL: American Institute of Steel Construction, p. 676.
- Attalla, M. R., G. G. Deierlein, and W. McGuire (1994). “Spread of plasticity: Quasi-plastic-hinge approach”. *Journal of Structural Engineering* 120.8, pp. 2451–2473.
- Duan, L. and W.F. Chen (1990). “A yield surface equation for doubly symmetrical sections”. *Engineering Structures* 12.2, pp. 114–119.
- ECCS (1984). “Ultimate limit state calculation of sway frames with rigid joints”. *TC 8 of European Convention for Constructional Steelwork (ECCS)* No. 33.
- Galambos, T. V. and R. L. Ketter (1959). “Columns under combined bending and thrust”. *Journal of the Engineering Mechanics Division* 85.2, pp. 1–30.
- Ge, X. and J.A. Yura (2019). “The strength of rotary-straightened steel columns”. *Proceedings of the 2019 SSRC Annual Stability Conference*. St. Louis, MO.
- Kucukler, M., L. Gardner, and L. Macorini (2014). “A stiffness reduction method for the in-plane design of structural steel elements”. *Engineering Structures* 73, pp. 72–84.
- Rosson, B.T. (2017). “Major and minor axis stiffness reduction of steel beam-columns under axial compression and tension conditions”. *Proceedings of the 2017 SSRC Annual Stability Conference*. San Antonio, TX.
- Rosson, B.T. (2018). “Modeling the Influence of Residual Stress on the Ultimate Load Conditions of Steel Frames”. *Proceedings of the 2018 SSRC Annual Stability Conference*.
- Rosson, B.T. (2021). “Beam element material models for straightened hot rolled sections and welded HSS sections”. *Proceedings of the 2021 SSRC Annual Stability Conference*. St. Louis, MO.
- Rosson, B.T. and R.D. Ziemian (2019). “Validation study of a new inelastic material model for steel W-Shapes”. *Proceedings of the 2019 SSRC Annual Stability Conference*. St. Louis, MO.
- Santathadaporn, S. and W.F. Chen (1970). *Interaction curves for sections under combined biaxial bending and axial force*. Welding Research Council.
- Schaper, L. et al. (2022). “A novel residual stress model for welded I-sections”. *Journal of Constructional Steel Research* 188, p. 107017.
- Ziemian, R. D. and W. McGuire (2002). “Modified tangent modulus approach, a contribution to plastic hinge analysis”. *Journal of Structural Engineering* 128.10, pp. 1301–1307.
- Ziemian, R.D., W. McGuire, and S. Liu (2019). *MASTAN2 v5.1.20*.